Journal of Nuclear Medicine, published on October 19, 2017 as doi:10.2967/jnumed.117.200048

^{68}Ga-NOTA-functionalized Ubiquicidin: Cytotoxicity, Biodistribution, Radiation Dosimetry and First-in-Human Positron Emission Tomography/Computed Tomography Imaging of Infections

Thomas Ebenhan[1], Mike M. Sathekge[1#], Thabo Lengana[1], Michel Koole[2], Olivier Gheysens[2], Thavendran Govender[3] and Jan R. Zeevaart[4]

1) Department of Nuclear Medicine, University of Pretoria and Steve Biko Academic Hospital, Pretoria, South Africa

2) Nuclear Medicine and Molecular Imaging, University Hospitals Leuven, Leuven, Belgium

3) Catalysis and Peptide Research Unit, University of KwaZulu-Natal, Durban, South Africa

4) Department of Science and Technology, Preclinical Drug Development Platform, North West University, Potchefstroom, South Africa

Short Title: ^{68}Ga-NOTA-UBI: imaging of infection

[#]Corresponding Author:
Professor Mike Sathekge
Head of Nuclear Medicine: University of Pretoria & Steve Biko Academic Hospital
Tel: +27 12 354 1794
Fax: +27 12 345 1219
Email: mike.sathekge@up.ac.za or sathekgemike@gmail.com

ABSTRACT

Ubiquicidin is an antimicrobial peptide (AMP) with great potential for nuclear imaging of infectious diseases as its cationic-rich fragment TGRAKRRMQYNRR (UBI) has been functionalized with 1,4,7-triazacyclononane-1,4,7-triacetic acid (NOTA) to allow complexation to Gallium-68 (^{68}Ga-NOTA-UBI). We herein assess the cytotoxicity, radiation dosimetry for ^{68}Ga-NOTA-UBI and a first-in-human evaluation to diagnose infectious processes. **Methods:** Cytotoxicity was evaluated in green monkey kidney epithelial (Vero) cells and MT-4 leucocytes. Tracer susceptibility was studied *in vitro* using different bacterial and fungal strains. Positron Emission Tomography-Computed Tomography (PET-CT)-based biodistribution, pharmacokinetics and radiation dosimetry were carried out in non-human primates (NHP). Two healthy volunteers and three patients with suspected infection underwent ^{68}Ga-NOTA-UBI-PET-CT imaging. **Results:** Negligible cytotoxicity was determined for NOTA-UBI. ^{68}Ga-NOTA-UBI showed moderate blood clearance (29 min half-life) and predominant renal clearance in NHP. Human radiation dose estimates indicated the bladder wall as the dose-critical tissue (185 µSv/MBq) followed by kidneys (23 µSv/MBq). The total absorbed body dose was low (<7 µSv/MBq); the effective dose was estimated at 17 µSv/MBq. ^{68}Ga-NOTA-UBI was capable to diagnose bone- and soft-tissue infection in 3/3 patients. **Conclusion:** ^{68}Ga-NOTA-UBI is considered a non-toxic, safe-to-administer radiopharmaceutical unlikely to cause adverse effects in humans. The favorable tracer biodistribution and the first-in-human results will make ^{68}Ga-NOTA-UBI-PET-CT an encouraging future diagnostic technique with auxiliary clinical relevance.

KEY WORDS

Gallium-68; ubiquicidin; UBI29-41; PET-CT-imaging; infection imaging; ^{68}Ga-NOTA-UBI(29-41); ^{68}Ga-UBI; dosimetry, imaging of infection

INTRODUCTION

Conventionally, bacterial infections are diagnosed by clinical examination, characteristic symptoms and culturing of microorganisms from blood, urine or sputum samples. Radiological techniques, such as ultrasound or CT may be helpful but are not always able to differentiate septic from aseptic processes and only identify anatomical changes related to late stage infections while Magnetic Resonance Imaging (MRI) cannot be applied in patients suffering from claustrophobia or bearing implanted medical devices.

Scintigraphy and PET can track radiolabeled leukocyte infiltration into the infection site using a whole-body imaging approach and allow for early detection of infectious areas well before anatomical changes occur (*1*). Approved radiopharmaceuticals to assess infectious diseases include *in vitro* or *in vivo* radiolabeled leukocytes, ^{18}F-fluorodeoxyglucose (^{18}F-FDG), ^{67}Ga-citrate, and radiolabeled antibodies targeting leukocyte antigens (*2*). However, these tracers show considerable variation in accuracy to diagnose infections (*3*). Therefore the development of bacteria-specific imaging probes is a promising alternative to more reliably detect infections (*4,5*). Radiolabeled antibiotics, vitamins, other biomimetics, AMP and bacteriophages have been highlighted as potential infection imaging agents (*6-10*).

AMP such as ubiquicidin are used as targeting vectors for molecular imaging because of their selectivity for bacterial cell membranes in the innate immune system response (*11*). Studies of cation-rich ubiquicidin fragments, including TGRAKRRMQYNRR (UBI) (*12*) have shown them to be useful as infection nuclear imaging agents. This peptide, directly labeled with technetium-99m (^{99m}Tc), shows preferential binding to bacterial rather than mammalian cells *in vitro* and allows identification of infected sites and better discrimination from the surrounding sterile or inflamed tissue in animals and human subjects (*13-15*). While Single-Photon Emission Computed Tomography is a widely available technique, PET may be superior in terms of its image resolution, sensitivity and quantification. Therefore a ^{68}Ga-radiolabeled PET derivative of UBI was developed, meeting the physiological half-life of peptides (*16*) and using a biological

targeting vector (i.e. peptide bioconjugates). Chelation with bi-functional chelator molecule NOTA (*17-19*) was used to conjugate UBI allowing for ^{68}Ga-radiolabeling (*20*). Upon radiosynthesis, a successful preclinical evaluation as a bacteria-selective imaging was approved in three different rabbit models (*21*). Before clinical applications, the safety of radiopharmaceuticals, to a certain extent, needs to be determined towards tolerability and possible side effects of the radiotracer (*22*). We therefore aimed to demonstrate that ^{68}Ga-NOTA-UBI can be used as a safe radiopharmaceutical for human applications by achieving results regarding its *in vitro* cytotoxicity, biodistribution and estimated human radiation dosimetry in NHP. In addition, we report the results of a first-in-human study on the imaging performance of ^{68}Ga-NOTA-UBI-PET-CT in patients with suspected infection.

MATERIALS AND METHODS

A supplement data file provides details for material and some methods (http://jnm.smnjournals.org).

$^{nat/68}$Ga-labeling of NOTA-UBI: NOTA-functionalized UBI was labeled “cold” with gallium(III)chloride ($^{nat}GaCl_3$) (for *in vitro* assays) or radiolabeled in a sterile, pyrogen-free fashion with ^{68}Ge/^{68}Ga generator-derived (iThemba LABS, Somerset West, South Africa) $^{68}Ga[Cl_4]^-$ (all *in vivo* applications) as described previously (*20*).

Cytotoxicity: Vero cells were utilized studying any noxious potential of NOTA, NOTA-UBI and ^{nat}Ga-NOTA-UBI according to a previously described method (*23*). Additionally, cytotoxicity to MT-4 leucocytes was determined by compound dose escalation or calculating the half-maximal inhibitory concentration (IC_{50}) (*24*).

Antibacterial and antifungal susceptibility: Bacterial susceptibility was determined using the broth micro-dilution method (*25*) on freshly cultured bacterial strains using a final working suspension of 10^6 cells/mL. The fungal susceptibility was evaluated in yeast strains by a method described elsewhere (*26*) using a working suspension of 5×10^3 cells/mL.

^{68}Ga-NOTA-UBI pharmacokinetics and tracer biodistribution in NHP: The study enrolled three NHP according to the South African code of practice for the care and use of animals. Ethical approval was given by the Pretoria University (Reference: H001-09). Adult vervet monkeys (*Chlorocebus aethiops*) were obtained from the Biomedical Research Centre (Onderstepoort, Pretoria University). Animals were handled as previously described (*27*). Image acquisition started 30, 60 and 120 min after intravenous administration of ^{68}Ga-NOTA-UBI using a PET-CT scanner (Biograph True Point 40-slice CT; Siemens/CTI, Knoxville, TN, USA). Arterial blood samples and urine were collected. Tissue and organ uptake were calculated as percentage of injected dose (%ID); tracer activity concentration was represented by standardized uptake value (SUV).

Dosimetric analyses in NHP: Radiation absorbed doses were calculated according to the Medical Internal Radiation Dose method (OLINDA/EXM 1.0) for internal dose assessment (*28*).

PET-CT imaging in humans: Two healthy volunteers and three patients with known/suspected infection were approved for this first-in-human study by the institutional Ethics Committee. Nuclear imaging was carried out using a previously published procedure (*27*).

Statistical Analyses: Results were expressed as mean and standard deviation (±SD) or standard error of mean (±SEM).

RESULTS

Cytotoxicity: Cytotoxicity was tested by escalating compound concentrations in Vero cells (**Supplement Fig. 1**) and by standard IC_{50} calculations in MT-4 leukocytes. Vero cells sustained cellular viability upon the maximum treatment concentration of 200 µM (P>0.05). The percentage of viable cells was calculated as 97.7 ± 4.1, 98.1 ± 2.1, 95.8 ± 3.7, 90.8 ± 8.3, and 96.6 ± 3.7 for UBI, NOTA-UBI, ^{nat}Ga-NOTA-UBI, ^{nat}Ga-NOTA, and the control, respectively. A significant cytotoxic response was found with 0.1-4 ppm $CdCl_2$ (positive control); the percentage of viable cells seemingly decreased with increasing $CdCl_2$ amounts (r^2=0.85). Thus, $CdCl_2$ caused significant differences in comparison to all tested compounds (P<0.01). Leukocytes exhibited no cytotoxicity; the normalized IC_{50} values (mM) were calculated as 340, 270, and 260 for UBI, NOTA-UBI, and ^{nat}Ga-NOTA-UBI respectively. No substantial leukocyte toxicity occurred upon treatment with the control (Indinavir, IC_{50}=301 nM).

Antimicrobial and antifungal susceptibility: None of the UBI derivatives tested appeared to exhibit substantial antibacterial or antifungal activity and cased insignificant inhibition of bacterial / fungal growth up to a maximum concentration (0.2 mg/mL), being 10000-fold higher than the tracer concentration considered in human blood following intravenous administration. In the same assay the minimal inhibitory concentrations (µg/mL) of neomycin were 0.32, 0.87, 2.0, and 32.6 for *S. aureus*, *B. subtilis*, *E. coli,* and *P. aeruginosa* respectively. The minimal inhibitory concentrations (µg/mL) determined for clotrimazole were 0.04, 0.03 and 1.0 for *C. albicans* 24433, *C. albicans* 90028, and *C. parasilopsis* respectively.

^{68}Ga-NOTA-UBI imaging, pharmacokinetics and biodistribution in NHP: NHP were injected with 33-45 MBq/kg ^{68}Ga-NOTA-UBI (244 ± 50 MBq - decay-corrected, specific activity 13.8 ± 1.9 GBq/µmol). A 3.5-6.5 mL saline bolus contained 29.7 ± 2.1 nmol NOTA-UBI (distributed as 72 ± 19 pmol/mL blood) (**Supplement Table 1**). Maximum image projection (MIP) PET-CT showed

early-onset tracer biodistribution with the highest tracer concentrations in the bladder, kidneys, liver and heart (**Fig. 1**). Significant tracer washout over 120 min was determined for blood, heart, spleen, lung, stomach, thyroid, bone, genitals and muscle. The SUV of all other organs were similar or lower than seen for the musculoskeletal tissue (**Supplement Table 2**). The time-activity curves resulting from blood and urine sampling are illustrating relatively rapid tracer blood clearance (2.64 %ID/h) (**Supplement Fig. 2**) and the distribution fitted an exponential function (29 min half-life, r^2=0.77; N=19; C_{max}=0.49 ± 0.19 %ID/g). The radioactivity was recovered predominately via the renal excretion route as follows: 15.4 %ID/h excretion rate, 74 ± 4 %ID cumulative percentage recovery voiding over 120 min, C_{max} = 39 ± 8 %ID (r^2=0.90; N=17).

Estimation of human absorbed doses by extrapolating data from ^{68}Ga-NOTA-UBI biodistribution in NHP: Human radiation doses represent the organ related burden to a normal sized adult. The extrapolated tracer biodistribution in humans based on ^{68}Ga-NOTA-UBI injection into NHP is summarized in **Supplement Table 3**. Absorbed doses (**Table 1**) were calculated from integrated organ residence times (**Supplement Table 4**). The effective dose was 17 ± 6 µSv/MBq, estimating a total human dose range between 3.1 and 4.3 mSv/tracer administration. Due to the dominant renal excretion route, the radioactive burden was the highest in the bladder wall and kidneys. Secondary critical organ was liver and lung. All other values were ≤10 µSv/MBq. A low total body dose of <7 µSv/MBq was absorbed.

PET-CT imaging in humans: Two 18 year-old healthy volunteers (m/f) and three patients (m/f/f; age range 34-69 years) with known/suspected bone- and/or soft-tissue infections received 174 ± 42 MBq (range: 129-240 MBq) ^{68}Ga-NOTA-UBI corresponding to 22.5 ± 3.8 nmol (range: 21.3-25.5 nmol) of NOTA-UBI (**Supplement Table 1**). Patients did not suffer from any acute adverse reaction such as altered blood pressure, rashes, itching, flushing, nausea,

coughing, muscle cramps or dizziness upon tracer injection (no long-term adverse effects were reported either). PET images showed tracer accumulation in kidneys and bladder, representing renal excretion (**Fig. 2**). Minimal radioactivity was noted in liver and myocardium (including vasculature system). The tracer concentration (N=5; SUV_{mean} ± SD) for heart, lung, liver, spleen, kidneys, urinary bladder and muscle tissue were respectively 2.3 ± 0.4, 0.57 ± 0.09, 1.8 ± 0.8, 1.4 ± 0.5, 11 ± 8, 21 ± 6, and 0.32 ± 0.05. In 3/3 patients (100%), ^{68}Ga-NOTA-UBI-PET-CT accurately identified the infectious area that have also been confirmed by other techniques. All ^{68}Ga-NOTA-UBI-PET images showed a significantly higher SUV at the infection site than the respective reference tissues ($P< 0.05$) resulting in high target-to-background ratios and good delineation of the infectious regions. A representative image of two patients with acute / chronic osteomyelitis in the ankle joint and an extending soft tissue infection into the legs, confirmed by radiography and bone scintigraphy is shown (**Fig. 3**). **Figure 4** shows a spinal infection in a 69-year-old patient which was confirmed by MRI and further clinical testing. The SUV_{max} in the infection sites was 3.3 ± 0.3 and the SUV_{mean} of infected tissue was 3.1-3.6-fold higher compared to the contralateral, uninfected tissue ($P< 0.001$).

DISCUSSION

Novel approaches have been proposed and made to conquer challenges in imaging infectious diseases, including discriminating infection from sterile inflammation, spread of infection and therapy monitoring (*5,29*). It is known that even slight modifications of a molecule may significantly alter its biological properties, hence necessitating evaluation of any tracer derivative to determine its efficacy and safety prior to human administration (*30,31*).

Toxicity: Our *in vitro* testing showed minimal cellular toxicity to cultured Vero cells suggesting negligible toxicity to patients. Moreover, the antimicrobial activity against selected bacterial and fungal strains showed minimal toxicity which is expected since it would be counter-productive

for AMP. They are naturally found in human bodies and other mammals, and never exhibit significant toxicity towards the organism's host cells (*7,32,33*). The lack of antimicrobial activity is advantageous for this diagnostic agent because killing of the targeted bacteria could result in trafficking of dead pathogens and the attached tracer to remote sites, thereby distorting the image and interpretation as to the extent of the infectious focus (*32,34*). The observed lack of antimicrobial activity was in contradiction with the results of Brouwer *et al*. (*22*). UBI has been reported to exhibit noteworthy toxicity against methicillin-resistant *Staphylococcus aureus*; however, a non-methicillin-resistant, laboratory staphylococcal strain and different methods were used in this study. AMP susceptibility to methicillin-resistant *Staphylococcus aureus* was also proven for other peptides (*35*). Despite the lacking susceptibility, an uncompromised bacterial binding affinity was reported for ^{68}Ga-NOTA-UBI (*6,20,36*). Lupetti *et al.* (*37*) studied the antifungal activity of UBI against *Aspergillus fumigates hyphae* and reported an IC_{50} concentration of 0.15 ± 0.03 mg/mL. Although the fungi species was different, antifungal activity against *Aspergillus fumigates* and *Candida* spp. was minimal. As with antibacterial activity, antifungal activity is not required but unabridged binding affinity is desired for radiodiagnostic agents facilitating infection imaging.

^{68}Ga-NOTA-UBI imaging and dosimetry: As an AMP, UBI was expected to be non-immunogenic and considered non-toxic, which initially fast tracked its evaluation for scintigraphic imaging (*38*). ^{99m}Tc-UBI29-41 was administered to humans to study pharmacokinetics following tracer injection *in vivo* (*39*). Thereafter, the first-in-human study enrolled patients with infection of the bone, soft-tissue, or prostheses. No adverse effects occurred following ^{99m}Tc-UBI29-41 imaging of the infectious scenarios (*14*). Recently, we have shown that NOTA conjugation of UBI29-41 did not compromise the targeting ability of this AMP fragment to selectively bind to the bacterial cell envelope (*20*). At present, no published study focused on the safe administration of ^{68}Ga-NOTA-UBI and its translation into clinical

applications. We were able to generate initial findings during a proof-of principle investigation where ^{68}Ga-NOTA-UBI was safely administered to rabbits bearing muscular infection paired with a contralateral sterile inflammation site (*21*). Similar results from another research group support our findings using infected mice. The tracer was found stable in PBS and blood samples (*36,40*). All animals seem to have tolerated the tracer injections well; it seems safe to conclude that there is a negligible risk concerning the administration of ^{68}Ga-NOTA-UBI.

Herein, we demonstrated radiation dosimetry estimates in NHP translatable to human applications of ^{68}Ga-NOTA-UBI. These should be considered preliminary results based on a setup with three male vervet monkeys undergoing ^{68}Ga-NOTA-UBI-PET-CT to study blood clearance, tissue biodistribution, tracer excretion and estimation of radiation doses. The vervet monkey biomedical model is reported to suit several investigations such as behaviourism, metabolism and immunity (*41*). The similar blood distribution volume to humans (60-70 mL/kg) make NHP models ideal to translate advanced radiopharmaceuticals into humans as they can provide significant information regarding tracer biodistribution or dosimetry. The bolus injection, activity concentration, specific activity and total peptide mass injected in NHP mimicked those considered for human application, yet the lower body weight of the monkeys increased the administered dose by 15-fold as compared to human doses. The study design included simple access to blood and urine samples which allowed meeting statistical compliance in a small number of animals compared to rodents. The pharmacokinetics showed the desired radioactivity blood clearance over 60 min p.i. (P<0.001). Based on this result, the first-in-human investigations, presented herein, were set for static imaging at 60 min after tracer injection. As an advantage, the lacking hepatobiliar tracer excretion may suggest ^{68}Ga-NOTA-UBI-PET for diagnostic of abdominal infection. The overall radiation dose and the dose to regenerative tissues such as red marrow, osteogenic cells, ovaries and gonads were favourably low (<10 μSv/MBq). Since the scope of the study allowed only for male monkeys, radiation dose estimates for ovaries, uterus and breasts relied on the assumption that the tracer biodistribution

is similar for women and men. The bladder was voided in order to create urine samples and to mimic the clinical setup where the patients void the bladder ahead of imaging. The human dose range was calculated as 3.1-4.3 mSv per ^{68}Ga-NOTA-UBI administration which adheres well to the guidelines regarding the maximum exposure for a single radioactive injection in Europe (10 mSv) (*42*). No comparative dosimetry of other ^{68}Ga-labeled infection imaging agents is currently available. The radiation dose for one ^{68}Ga-NOTA-UBI dose is significantly lower than considered for ^{18}F-FDG ($P<0.05$) and 3.5-times less than the radiation dose of ^{68}Ga-DOTA-TATE, another diagnostic ^{68}Ga-tracer used in humans (*43,44*).

PET-CT imaging in humans: This first-in-human study evaluating the diagnostic performance of ^{68}Ga-NOTA-UBI-PET-CT was performed in three patients with known/ suspected bone-or soft tissue infection. Except for the renal clearance and excretion, biodistribution in humans was similar to NHP and no significant differences were observed between healthy volunteers and patients with the exception of tracer accumulation in the infectious area. The accumulation of ^{68}Ga-NOTA-UBI over 60 min was sufficient to delineate the infectious tissues, as shown by a target-to-nontarget ratio of 3.4 ± 0.2 which is significantly higher ($P<0.05$) than reported values for ^{99m}Tc-UBI29-41 (2.3 ± 1.3; N=18) or ^{99m}Tc-HYNIC-UBI29-41 (1.9 ± 0.3; N=5) (*14,45*). Our pilot study demonstrates the capability of this imaging technique to detect infected tissues as confirmed by other techniques. Based on this targeting approach, tracer uptake is reflected by the bacterial burden rather than inflammatory cell influx as observed with PET imaging using ^{18}F-FDG or radiolabeled leucocytes. We described previously that the NOTA-UBI uptake follows an exponential dependence ($R^2>0.66$) with rising amounts of bacteria (gram$^{+/-}$) residing in the infection site (*46*). Similar to NOTA-UBI, the novel bacteria-specific PET-probe 2-fluoro-^{18}F-desoxysorbitol was developed in mice, tested recently in healthy volunteers, and is expected to diagnose enterobacteriaceae-specific infection in humans (*47,48*). The host-independent

targeting mechanism of UBI could qualify ^{68}Ga-NOTA-UBI-PET-CT as imaging modality to facilitate future differential diagnostics of infectious diseases.

Study scope and limitations: Some limitations of this study included that tracer pharmacokinetics, biodistribution, and dosimetry data were obtained from anaesthetized NHP which could affect the hemodynamics of various organs and may affect tracer uptake. Although the blood flow to the liver is altered less by isoflurane than by other anaesthesia methods, renal blood flow and urine production are decreased by isoflurane in mice (*49*). General anaesthesia could also affect the metabolism of ^{68}Ga-NOTA-UBI, similar to a significant reduction in brain glucose metabolism observed with ^{18}F-FDG (*50*). This study only allowed for three male NHP, which has limited statistical power and assumptive information on radiation burden in females. Due to the avid urinary tracer excretion, inferior imaging of urinary tract infections or infections in the pelvis (surrounding the bladder) may occur. However; favorable renal excretion was seen in human subjects than in NHP. Also, administering diuretics, bladder voiding or catheterization can significantly lower the dose to the bladder wall. Even though there is a major advantage of using radiolabeled AMP (they retain at the site of infection by internalization and subsequent amplification) imaging of phagocytosed microorganism may be limited (*13*) which can result in an underestimation of the actual bacterial burden.

CONCLUSION

This study demonstrates that ^{68}Ga-NOTA-UBI is a non-toxic, safe-to-administer radiopharmaceutical unlikely to cause adverse effects in humans. Biodistribution corresponds to major peptide-metabolizing organs and predominantly urinary excretion. ^{68}Ga-NOTA-UBI-PET-CT was able to accurately identify all infectious foci in the three patients with suspected infection. Even though the first-in-human results are encouraging, further clinical studies are required to assess the diagnostic accuracy of ^{68}Ga-NOTA-UBI for imaging infectious diseases.

COMPLIANCE WITH ETHICAL STANDARD

- All authors declare no conflicts of interest.
- This study was performed in accordance with the ethical standard of our institution and with the 1964 Helsinki Declaration and its later amendments.
- Informed consent was obtained from all patients.

ACKNOWLEDGMENTS

Financial support was given by the Nuclear Technologies in Medicine and the Biosciences Initiative, managed by Necsa and funded by the DST. The authors thank Dr. Parboosing for contributing to all cellular assays, Dr. Naidoo and Dr. Pulker for NHP surveillance, Dr. Modiselle for recruiting the healthy volunteers / patients, and Mrs. van Wyk for assisting with image acquisition.

REFERENCES

1. Goldsmith SJ, Vallabhajosula S. Clinically proven radiopharmaceuticals for infection imaging: mechanisms and applications. *Semin Nucl Med.* 2009;39:2-10.

2. Boerman OC, Dams ET, Oyen WJ, Corstens FH, Storm G. Radiopharmaceuticals for scintigraphic imaging of infection and inflammation. *Inflamm Res.* 2001;50:55-64.

3. Sathekge M, Maes A, D'Asseler Y, Vorster M, Van de Wiele C. Nuclear medicine imaging in tuberculosis using commercially available radiopharmaceuticals. *Nucl Med Commun.* 2012;33:581-590.

4. Signore A, D'Alessandria C, Lazzeri E, Dierckx R. Can we produce an image of bacteria with radiopharmaceuticals? *Eur J Nucl Med Mol Imaging.* 2008;35:1051-1055.

5. Bunschoten A, Welling MM, Termaat MF, Sathekge M, van Leeuwen FW. Development and prospects of dedicated tracers for the molecular imaging of bacterial infections. *Bioconjugate Chem.* 2013;24:1971-1989.

6. Signore A, Chianelli M, D'Alessandria C, Annovazzi A. Receptor targeting agents for imaging inflammation/infection: where are we now? *Q J Nucl Med Mol Imaging.* 2006;50:236-242.

7. Lupetti A, Nibbering PH, Welling MM, Pauwels EK. Radiopharmaceuticals: new antimicrobial agents. *Trends Biotechnol.* 2003;21:70-73.

8. Basu S, Chryssikos T, Moghadam-Kia S, Zhuang H, Torigian DA, Alavi A. Positron emission tomography as a diagnostic tool in infection: present role and future possibilities. *Semin Nucl Med.* 2009;39:36-51.

9. Kumar V, Boddeti DK. ^{68}Ga-radiopharmaceuticals for PET imaging of infection and inflammation. *Recent Results Cancer Res.* 2013;194:189-219.

10. Sathekge M. The potential role of ^{68}Ga-labeled peptides in PET imaging of infection. *Nucl Med Commun.* 2008;29:663-665.

11. Ebenhan T, Gheysens O, Kruger HG, Zeevaart JR, Sathekge MM. Antimicrobial peptides: their role as infection-selective tracers for molecular imaging. *BioMed Res Int.* 2014;2014:867381.

12. Hiemstra PS, van den Barselaar MT, Roest M, Nibbering PH, van Furth R. Ubiquicidin, a novel murine microbicidal protein present in the cytosolic fraction of macrophages. *J Leukoc Biol.* 1999;66:423-428.

13. Nibbering PH, Welling MM, Paulusma-Annema A, Brouwer CP, Lupetti A, Pauwels EK. ^{99m}Tc-Labeled UBI29-41 peptide for monitoring the efficacy of antibacterial agents in mice infected with Staphylococcus aureus. *J Nucl Med.* 2004;45:321-326.

14. Akhtar MS, Qaisar A, Irfanullah J, et al. Antimicrobial peptide ^{99m}Tc-ubiquicidin 29-41 as human infection-imaging agent: clinical trial. *J Nucl Med.* 2005;46:567-573.

15. Brouwer CP, Sarda-Mantel L, Meulemans A, Le Guludec D, Welling MM. The use of technetium-99m radiolabeled human antimicrobial peptides for infection specific imaging. *Mini Rev Med Chem.* 2008;8:1039-1052.

16. Fani M, Andre JP, Maecke HR. ^{68}Ga-PET: a powerful generator-based alternative to cyclotron-based PET radiopharmaceuticals. *Contrast Media Mol Imaging.* 2008;3:67-77.

17. Velikyan I, Beyer GJ, Bergström-Pettermann E, Johansen P, Bergström M, Långström B. The importance of high specific radioactivity in the performance of ^{68}Ga-labeled peptide. *Nucl Med Biol.* 2008;35:529-536.

18. Velikyan I. Prospective of ^{68}Ga-radiopharmaceutical development. *Theranostics.* 2014;4:47-80.

19. Velikyan I. Positron emitting [^{68}Ga]Ga-Based imaging agents: chemistry and diversity. *Med Chem.* 2011;7:345-379.

20. Ebenhan T, Chadwick N, Sathekge MM, et al. Peptide synthesis, characterization and ^{68}Ga-radiolabeling of NOTA-conjugated ubiquicidin fragments for prospective infection imaging with PET/CT. *Nucl Med Biol.* 2014;41:390-400.

21. Ebenhan T, Zeevaart JR, Venter JD, et al. Preclinical evaluation of ^{68}Ga-labeled 1,4,7-triazacyclononane-1,4,7-triacetic acid-ubiquicidin as a radioligand for PET infection imaging. *J Nucl Med.* 2014;55:308-314.

22. Brouwer CP, Bogaards SJ, Wulferink M, Velders MP, Welling MM. Synthetic peptides derived from human antimicrobial peptide ubiquicidin accumulate at sites of infections and eradicate (multi-drug resistant) *Staphylococcus aureus* in mice. *Peptides.* 2006;27:2585-2591.

23. Pawar SA, Jabgunde AM, Govender P, et al. Synthesis and molecular modelling studies of novel carbapeptide analogs for inhibition of HIV-1 protease. *Eur J Med Chem.* 2012;53:13-21.

24. Mokaleng BB, Ebenhan T, Ramesh S, et al. Synthesis, ^{68}Ga-radiolabeling and preliminary in vivo assessment of a depsipeptide-derived compound as a potential PET/CT infection imaging agent. *BioMed Res Int.* 2015;2015:284354.

25. Eloff JN. A sensitive and quick microplate method to determine the minimal inhibitory concentration of plant extracts for bacteria. *Planta Med.* 1998;64:711-713.

25. Cuesta I, Bielza C, Cuenca-Estrella M, Larranaga P, Rodriguez-Tudela JL. Evaluation by data mining techniques of fluconazole breakpoints established by the Clinical and Laboratory Standards Institute (CLSI) and comparison with those of the European Committee on Antimicrobial Susceptibility Testing (EUCAST). *Antimicrob Agents Chemother.* 2010;54:1541-1546.

26. Ebenhan T, Schoeman I, Rossouw DD, et al. Evaluation of a flexible NOTA-RGD kit solution using gallium-68 from different ^{68}Ge/^{68}Ga-generators: pharmacokinetics and biodistribution in nonhuman primates and demonstration of solitary pulmonary nodule imaging in humans. *Mol Imaging Biol.* 2017;19:469-482.

27. Stabin MG, Sparks RB, Crowe E. OLINDA/EXM: the second-generation personal computer software for internal dose assessment in nuclear medicine. *J Nucl Med*. 2005;46:1023-1027.

28. Palestro CJ. Radionuclide imaging of osteomyelitis. *Semin Nucl Med.* 2015;45:32-46.

29. Blok D, Feitsma RI, Vermeij P, Pauwels EJ. Peptide radiopharmaceuticals in nuclear medicine. *Eur J Nucl Med.* 1999;26:1511-1519.

30. Rennen HJ, Corstens FH, Oyen WJ, Boerman OC. New concepts in infection/inflammation imaging. *Q J Nucl Med Mol Imaging.* 2001;45:167-173.

31. Brouwer CP, Wulferink M, Welling MM. The pharmacology of radiolabeled cationic antimicrobial peptides. *J Pharm Sci.* 2008;97:1633-1651.

32. Guani-Guerra E, Santos-Mendoza T, Lugo-Reyes SO, Teran LM. Antimicrobial peptides: general overview and clinical implications in human health and disease. *Clin Immunol.* 2010;135:1-11.

33. Welling MM, Hiemstra PS, van den Barselaar MT, et al. Antibacterial activity of human neutrophil defensins in experimental infections in mice is accompanied by increased leukocyte accumulation. *J Clin Invest.* 15 1998;102:1583-1590.

34. Welling MM, Brouwer CP, van 't Hof W, Veerman EC, Amerongen AV. Histatin-derived monomeric and dimeric synthetic peptides show strong bactericidal activity towards multidrug-resistant Staphylococcus aureus in vivo. *Antimicrob Agents Chemother.* 2007;51:3416-3419.

35. Vilche M, Reyes AL, Vasilskis E, Oliver P, Balter H, Engler H. ^{68}Ga-NOTA-UBI-29-41 as a PET tracer for detection of bacterial infection. *J Nucl Med.* 2016;57:622-627.

36. Lupetti A, van Dissel JT, Brouwer CP, Nibbering PH. Human antimicrobial peptides' antifungal activity against Aspergillus fumigatus. *Eur J Clin Microbiol Infect Dis.* 2008;27:1125-1129.

37. Ferro-Flores G, Arteaga de Murphy C, Pedraza-Lopez M, et al. In vitro and in vivo assessment of ^{99m}Tc-UBI specificity for bacteria. *Nucl Med Biol.* 2003;30:597-603.

38. Melendez-Alafort L, Rodriguez-Cortes J, Ferro-Flores G, et al. Biokinetics of ^{99m}Tc-UBI 29-41 in humans. *Nucl Med Biol.* 2004;31:373-379.

39. Bhatt J, Mukherjee A, Korde A, Kumar M, Sarma HD, Dash A. Radiolabeling and Preliminary evaluation of Ga-68 labeled NODAGA-Ubiquicidin fragments for prospective infection imaging. *Mol Imaging Biol.* 2017;19:59-67.

40. Jasinska AJ, Schmitt CA, Service SK, et al. Systems biology of the vervet monkey. *ILAR J.* 2013;54:122-143.

41. Verbruggen A, Coenen HH, Deverre JR, et al. Guideline to regulations for radiopharmaceuticals in early phase clinical trials in the EU. *Eur J Nucl Med Mol Imaging.* 2008;35:2144-2151.

42. Hartmann H, Freudenberg R, Oehme L, et al. Dosimetric measurements of ^{68}Ga-high affinity DOTATATE: twins in spirit - part III. *Nuklearmedizin.* 2014;53:211-216.

43. Deloar HM, Fujiwara T, Shidahara M, Nakamura T, Yamadera A, Itoh M. Internal absorbed dose estimation by a TLD method for ^{18}F-FDG and comparison with the dose estimates from whole body PET. *Phys Med Biol.* 1999;44:595-606.

44. Gandomkar M, Najafi R, Shafiei M, et al. Clinical evaluation of antimicrobial peptide [^{99m}Tc/Tricine/HYNIC^{0}]ubiquicidin 29-41 as a human-specific infection imaging agent. *Nucl Med Biol.* 2009;36:199-205.

45. Ebenhan T, Venter JD, Maguire GEM, et al. Novel radiopharmaceutical and preclinical aspects of Ga-68-UBI: a selective PET tracer for imaging of infection. *In:*Third Theragnostics World Congress on Gallium-68 and PRRT: Abstracts. *J Nucl Med.* 2015;56(Suppl 2):2-30.

46. Zhu W, Yao S, Xing H, et al. Biodistribution and radiation dosimetry of the Enterobacteriaceae-specific imaging probe [^{18}F]Fluorodeoxysorbitol determined by PET/CT in healthy human volunteers. *Mol Imaging Biol.* 2016;18:782-787.

47. Weinstein EA, Ordonez AA, Demarco VP, et al. Imaging Enterobacteriaceae infection in vivo with ^{18}F-fluorodeoxysorbitol positron emission tomography. *Sci Transl Med.* 2015;6:259ra146.

48. Fueger BJ, Czernin J, Hildebrandt I, et al. Impact of animal handling on the results of ^{18}F-FDG PET studies in mice. *J Nucl Med.* 2006;47:999-1006.

49. Alstrup AK, Smith DF. Anaesthesia for positron emission tomography scanning of animal brains. *Lab Anim.* 2013;47:12-18.

50. Akhtar MS, Imran MB, Nadeem MA, Shahid A. Antimicrobial peptides as infection imaging agents: better than radiolabeled antibiotics. *Int J Pept.* 2012;2012:965238.

FIGURE LEGENDS (+ figures in reduced resolution)

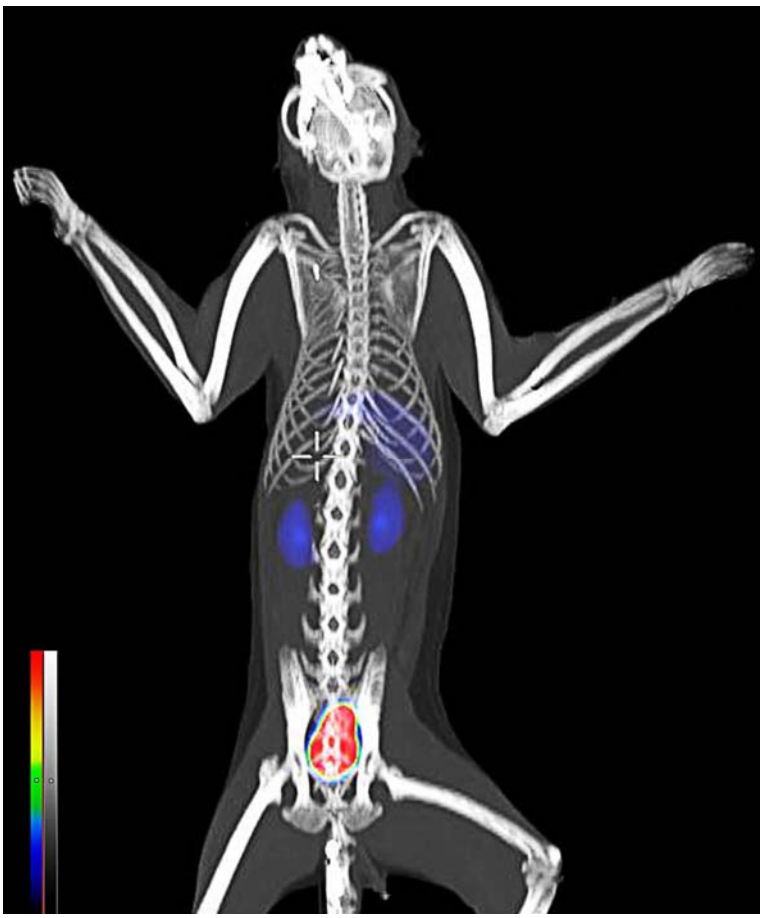

FIGURE 1.
Representative ^{68}Ga-NOTA-UBI-PET-CT biodistribution in a NHP 60 min after tracer administration (189 MBq)

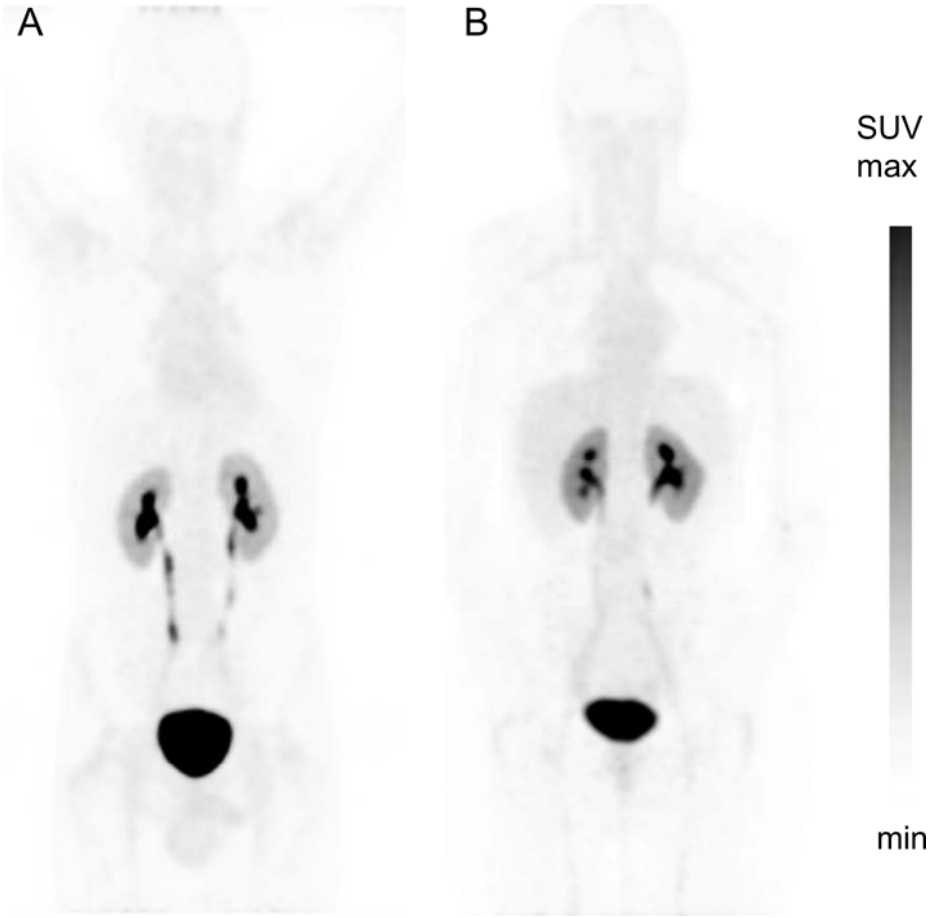

FIGURE 2. ^{68}Ga-NOTA-UBI-PET MIP image (skull to mid-thigh) demonstrating physiological tracer biodistribution in a healthy (**A**) male and (**B**) female volunteer. Images were acquired 60 min after intravenous injection of 132 MBq (♀) and 129 MBq (♂) tracer.

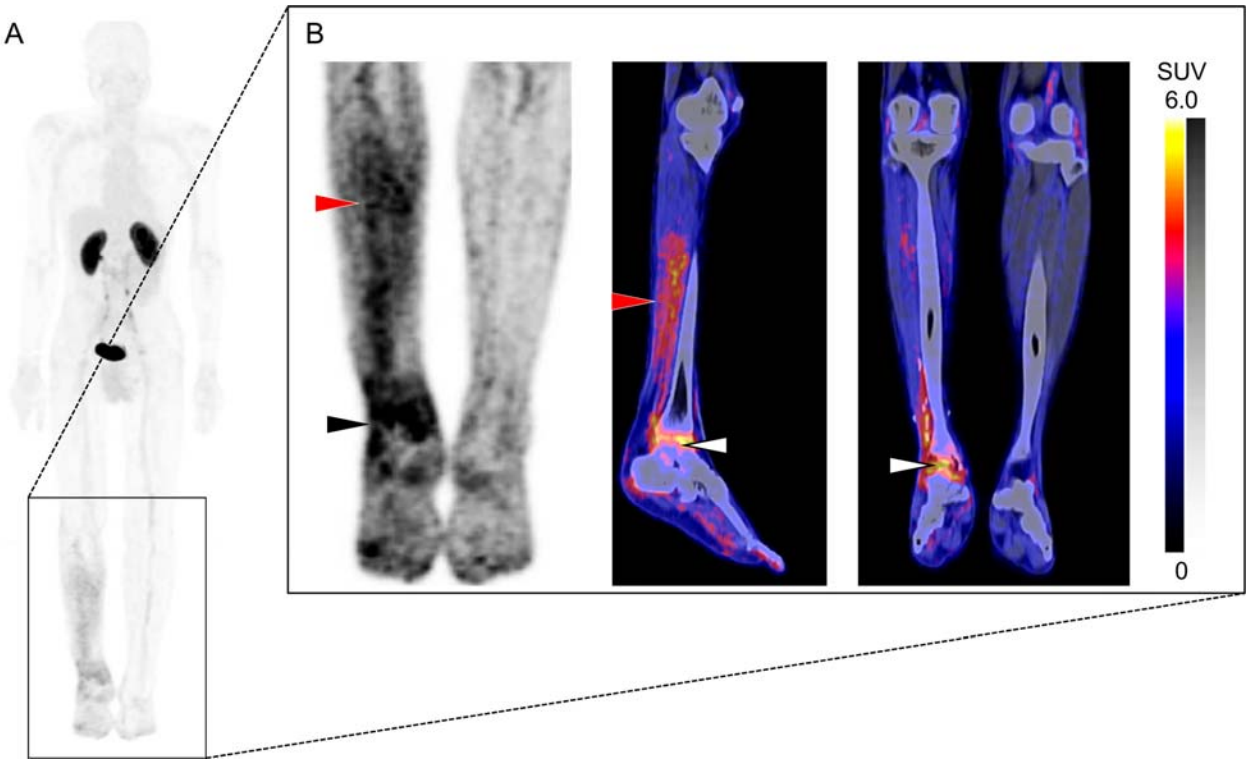

FIGURE 3. Representative ^{68}Ga-NOTA-UBI-PET-CT image in a patient with peripheral bone- and soft-tissue infection. **(A)** Whole-body MIP-PET image shows a diffusely increased tracer uptake in the right lower leg. (**B**) Detailed PET-CT images demonstrate focal increased tracer uptake in the ankle-joint extending in the adjacent bone (black and white arrows) as well as diffuse tracer uptake in the calf muscles (red arrow) whereas there is no significant uptake in the contralateral leg. Images are obtained 60 min after tracer administration (240 MBq)

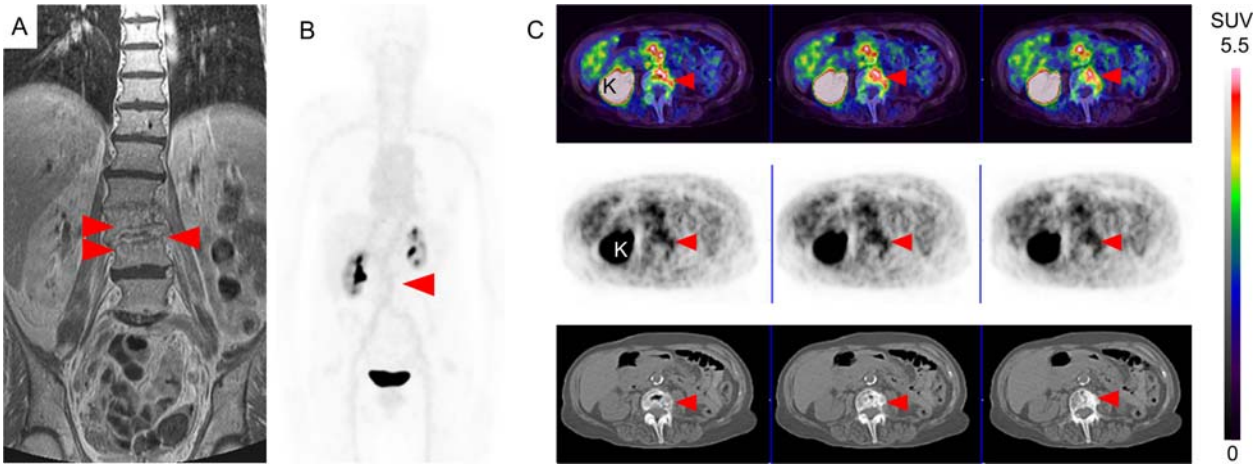

FIGURE 4. Representative MRI and ^{68}Ga-NOTA-UBI-PET-CT imaging in a patient with suspected spinal infection (spondylodiscitis). (**A**) Coronal T1 weighted MRI image (fat suppression), (**B**) whole-body MIP-PET image, and (**C**) sequential transaxial fused PET-CT (*top*), PET (*middle*) and CT (*bottom*) images showing focal increased uptake in the intervertebral region of L3-L4 corresponding to the abnormal findings on MRI. K=kidney.

TABLES

TABLE 1

Extrapolated Human Radiation Dose Estimates for ^{68}Ga-NOTA-UBI

Organ	Dose (μSv/MBq)	%CV
Adrenals	6.21	5.0
Brain	1.16	9.5
Breast	4.95	7.4
Gallbladder wall	6.84	5.5
Lower left intestine	8,50	15.5
Small intestine	7.58	7.0
Stomach wall	6.56	2.4
Upper left intestine	7.28	6.9
Heart wall	10.0	6.8
Kidneys	23.1	19.0
Liver	17.7	27.9
Lung	11.7	13.3
Muscle	3.70	9.7
Ovaries	7.60	10.0
Pancreas	6.15	21.0
Red marrow	6.67	5.6
Osteogenic cells	9.64	5.8
Skin	4.59	5.2
Spleen	7.67	15.5
Testes	5.01	25.6
Thymus	5.35	6.7
Thyroid	3.55	4.5
Urinary bladder wall	185	58.6
Uterus	10.3	22.2
Total Body	6.84	0.6

MATERIAL

Media, chemicals and equipment: Solvents, reagents, drugs and culture media were purchased from commercial sources in highest purity and used as recommended. NOTA-UBI was purchased from GL Biochem Ltd. (Shanghai, China). To determine mammalian cell toxicity, an automated PowerWave XS2 microplate reader (Biotek Instruments, Winooski, VT, USA) measuring optical density (OD), was utilized.

Bacteria, fungi and laboratory animals: Vero cells and MT-4 human leukocytes from LGC Standards (Johannesburg, South Africa) were used to assess *in vitro* cytotoxicity. Bacterial cells (*Escherichia coli (*ATCC 25922), *Staphylococcus aureus (*ATCC 25923), *Pseudomonas aeruginosa (*ATCC 27853), *Bacillus subtilis (*ATCC 6051)) and fungi (*Candida albicans (*ATCC 24433), *Candida albicans (*ATCC 90028) and *Candida parasilopsis (*ATCC 22019)) were obtained from the National Health Laboratory Services (Inkosi Albert Luthuli Hospital, Durban, South Africa) to test for compound susceptibility.

METHODS

Antibacterial and antifungal susceptibility: Freshly-cultured bacterial strains were suspended to 10^6 cells/mL; the yeast working suspension was adjusted to 1-5×10^3 cells/mL using a mixture containing RPMI (with L-glutamine, without bicarbonate) (Cambrex Bio Science, Verviers, Belgium) and 0.165 M morpholine propane sulfonic acid (MOPS) (Sigma-Aldrich, Germany) buffered to pH 7.0. NOTA, NOTA-UBI, ^{nat}Ga-NOTA and ^{nat}Ga-NOTA-UBI were dissolved in 10 % acetonitrile. Clotrimazole (0.0012 - 80 µg/mL) and Neomycin (both, Sigma, Germany) (0.0015 - 100 µg/mL) were used as reference drugs.

Dosimetric analyses: The following organs (heart, liver, spleen, lung, brain, thyroid, stomach, bone (femur), testes, muscle, pancreas, small and large intestines, kidneys and urinary bladder)

were identified as source organs and delineated. From these delineations, %ID per volume was determined and converted to %ID for humans using the following conversion formula:

$$\left(\frac{\%ID}{vol_{organ}} w_{body}\right)_{NHP} \left(\frac{vol_{organ}}{w_{body}}\right)_{Human} = \%ID_{Human}$$

Organ weights and whole-body weight of the male human phantom were used as representative values and converted to volume values using density values of 1.04, 1.40 and 0.296 g/cm^3 for soft tissue, bone and lungs respectively. Blood activity was assumed to be the same as for red marrow. Heart wall and heart content were included in the organ volume. Volumes of the intestinal tract and the urinary bladder contents were included but not the organ walls. For the different sub-organs, the activity was weighted based on the relative volumes. Finally, the %ID of the remainder was determined such that the total %ID adds up to 100%.

PET-CT imaging in humans: A brief description of the patient characteristics:1) A 37-year-old male patient presented with a suspicion of unilateral (right) ankle joint infection and osteomyelitis (OM), which was suggested on a prior bone scintigraphy. He presented with recurring leg pain suspicious for infectious spread into the surrounding soft tissue and calf muscle. Biochemical inflammatory parameters were significantly increased.

2) A 34-year-old female patient was diagnosed with septic OM in the right ankle based ^{99m}Tc-WBC scintigraphy. She presented with recurring pain and swelling in the ankle joint and drainage of serosanguinous fluid.

3) A 69-year-old female patient with a history of discitis presented with worsening pain and increased inflammatory parameters (ESR=16 mm/hr, CRP=105, white cell count= 6.45 x 10^9/L). CT-scan showed end-plate sclerosis from L2-L4 with wedge shaped volume loss of L3/L4. A prior MRI confirmed a L2/3 to L3/4 spondylodiscitis with significant erosion and collapse of the vertebral bodies with features suggestive of pyogenic spondylodiscitis/spondylitis.

Whenever possible, blood cultures and bacteriology were carried out to confirm the presence of infection. The results of clinical tests, radiography and bone scintigraphy were used in cases in which culturing of tissue samples could not be performed.

Statistical Analyses: Experiments were performed in triplicate unless otherwise stated. Where indicated, representative data from individual experiments are shown. Statistical significance was determined using the Student-*t* test (paired and unpaired). A value of (*) $P<0.05$, (**) $P<0.01$ and (***) $P<0.001$ were considered statistically significant.

RESULTS

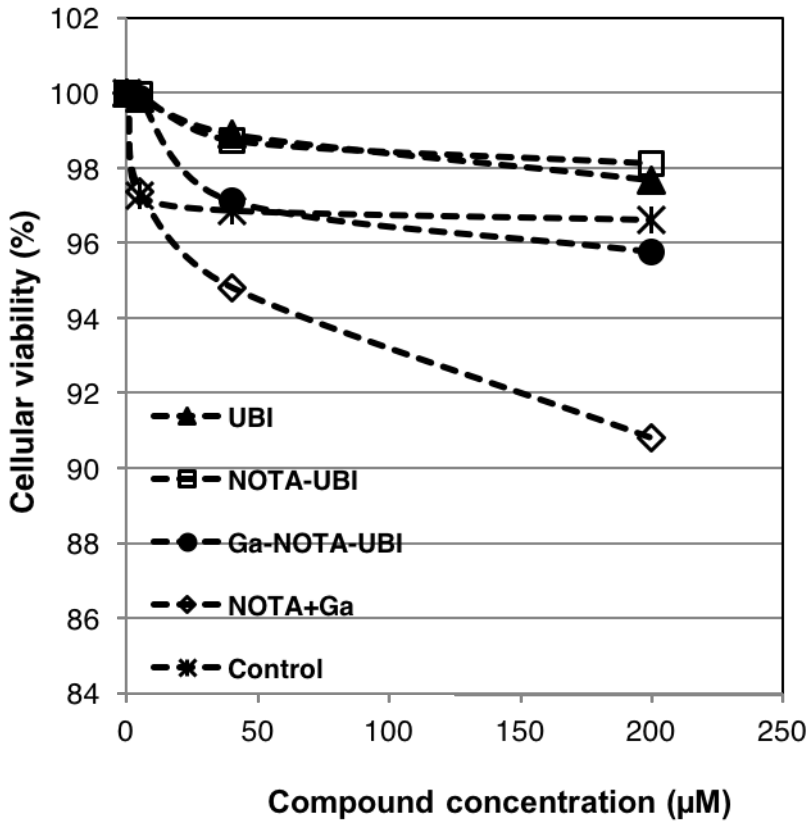

SUPPLEMENT FIGURE 1.

Cellular toxicity of ubiquicidin peptide derivatives in Vero cells. Average values across five replicates are presented. Standard error of mean display was omitted due to clarity (0.4-3.7% at 5 µM, 1.0-4.5% at 40 µM, 0.9-8.3% at 200 µM). UBI: ubiquicidin fragment 29-41; NOTA-UBI: NOTA-functionalized ubiquicidin fragment 29-41; Ga-NOTA-UBI: NOTA-functionalized ubiquicidin fragment 29-41 complexed with ^{nat}Ga; Ga+NOTA: NOTA complexed with ^{nat}Ga; Control: peptide coded GDEAEEMQYNEE (i.e. a negatively charged UBI fragment - any arginine (cationic charge) are replaced by aspartic acid (anionic charge)).

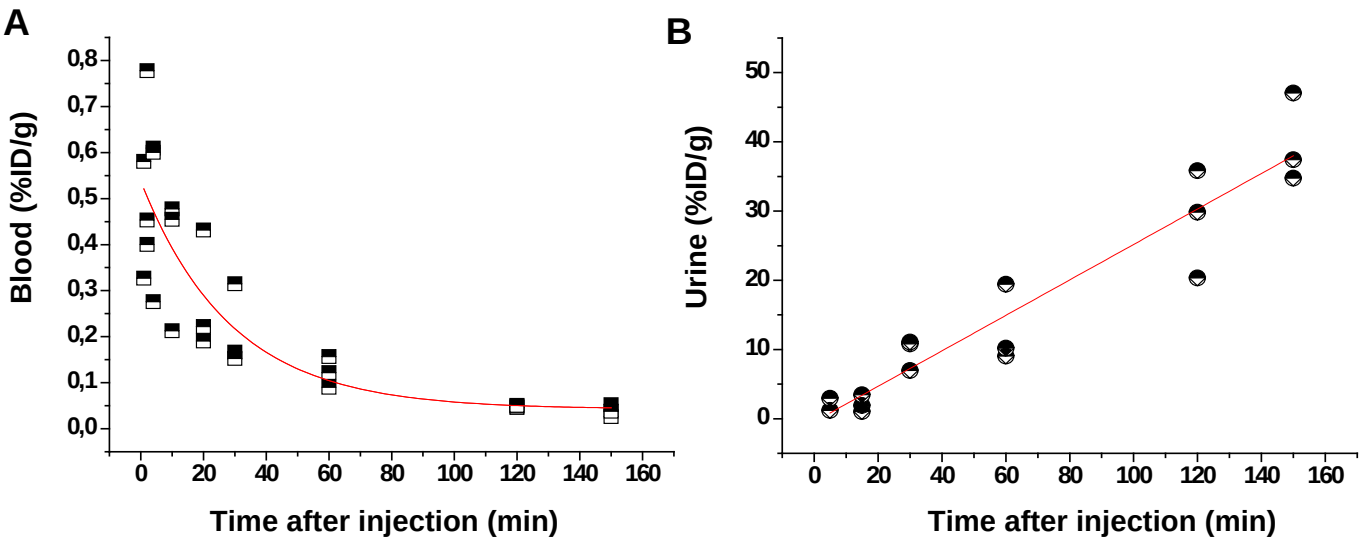

SUPPLEMENT FIGURE 2.

Time-dependent activity concentration of ^{68}Ga-NOTA-UBI showing blood clearance (**A**) and urine recovery (**B**) calculated from samples yielded from three vervet monkeys. Animals were injected intravenously with 38.9 ± 6.2 MBq/kg bodyweight. Data from available blood follows an exponential decline ($y=0.424e^{-0.017x}$; r^2= 0.877, N=19). Data from urinary activity recovery shows a linear incline ($y=0.252x$; r^2=0.904, N=17).

SUPPLEMENT TABLE 1.

Comparison of ^{68}Ga-NOTA-UBI Application in NHP and Humans

Characteristic	Vervet Monkeys*	Human†
Age (y); Sex (m/f)	> 8; m	35 ± 19; m/f
Body weight (kg)	6.8 ± 1.6	68 ± 22
Administered activity (MBq)	227 ± 27	174 ± 42
Administered dose (MBq/kg)	39 ± 6	2.7 ± 0.8

*) Results are expressed as mean values (± sem) for N= 3.
†) Results are expressed as mean values (± sem) for N= 5.
f=female; m=male

SUPPLEMENT TABLE 2.

Image-guided Organ Activity Concentration of ^{68}Ga-NOTA-UBI in NHP

Organ /Tissue	Concentration (SUV)†		
	30 min	**60 min**	**120 min**
Blood (*arcus aortae*)	1.11 ± 0.15	0.81 ± 0.09*****	0.49 ± 0.05*****
Heart	1.22 ± 0.07	0.78 ± 0.11	0.43 ± 0.04******
Liver	3.12 ± 0.73	2.72 ± 0.87	2.42 ± 0.87
Spleen	1.26 ± 0.21	0.95 ± 0.25	0.79 ± 0.29*****
Lung	0.66 ± 0.09	0.43 ± 0.05*****	0.25 ± 0.03*****
Brain	0.09 ± 0.02	0.05 ± 0.01	0.04 ± 0.01
Thyroid	0.45 ± 0.03	0.29 ± 0.05	0.20 ± 0.07*****
Stomach	0.42 ± 0.08	0.33 ± 0.11	0.21 ± 0.08*****
Bone (femur)	0.36 ± 0.09	0.26 ± 0.02	0.17 ± 0.03*****
Genitals (testes)	0.51 ± 0.13	0.40 ± 0.10*****	0.29 ± 0.11******
Muscle (reference tissue)	0.31 ± 0.02	0.18 ± 0.02*****	0.12 ± 0.02*****
Pancreas	0.80 ± 0.27	0.47 ± 0.09	0.30 ± 0.02
Intestines (small & large)	0.40 ± 0.19	0.28 ± 0.04	0.16 ± 0.02
Kidneys	4.67 ± 0.88	3.56 ± 0.68	2.79 ± 0.12
Bladder, urinary tract	26.4 ± 16.3	49.0 ± 16.5	35.6 ± 20.9

†) Average standard uptake value (SUV_{mean}) quantification from PET-CT imaging; results are expressed as average SUV (± SEM) for N=3. Two-way paired Student-*t* tests were performed comparing values of 60/120 min to values of 30 min: (*****) P ≤0.05 and (******) P ≤0.01.

SUPPLEMENT TABLE 3.

Extrapolated Tracer Biodistribution in Humans based on ^{68}Ga-NOTA-UBI Injection into NHP

Organ / Tissue	Biodistribution (% ID/Gram)†		
	30 min	60 min	120 min
Red marrow	1.22 ± 0.17	0.64 ± 0.07*	0.21 ± 0.03*
Heart wall	0.37 ± 0,02	0.17 ± 0.03*	0.05 ± 0.01**
Heart	0.55 ± 0,02	0.26 ± 0.04*	0.08 ± 0.01**
Stomach	0.11 ± 0.02	0.06 ± 0.02*	0.02 ± 0.01*
Liver	5.80 ± 1.34	3.68 ± 1.23*	1.79 ± 0.66*
Spleen	0.23 ± 0.04	0.12 ± 0.03*	0.06 ± 0.02**
Lung	2.25 ± 0.31	1.06 ± 0.14*	0.35 ± 0.05*
Brain	0.13 ± 0.03	0.05 ± 0.01	0.02 ± 0.001*
Pancreas	0.07 ± 0.03	0.03 ± 0.01	0.01 ± 0.001
Thyroid	0.01 ± 0.001	0.004 ± 0.001*	0.002 ± 0.001**
Bone (Femur)	1.05 ± 0.26	0.56 ± 0.06	0.20 ± 0.04*
Genitals (Testes)	0.02 ± 0.01	0.01 ± 0.003*	0.04 ± 0.002*
Intestines	0.31 ± 0.14	0.16 ± 0.02	0.05 ± 0.01
Small intestine	0.16 ± 0.07	0.08 ± 0.01	0.03 ± 0.004
Upper left intestine	0.09 ± 0.04	0.05 ± 0.001	0.02 ± 0.003
Lower left intestine	0.06 ± 0.03	0.03 ± 0.004	0.01 ± 0.002
Kidneys	1.36 ± 0.25	0.76 ± 0.15	0.32 ± 0.02*
Bladder & urinary tract	5.4 ± 3.3	7.3 ± 2.3	2.9 ± 1.6
Remainder of body	47 ± 5	36 ± 2*	22 ± 2**

†) decay-corrected organ activity uptake in percentage of the total injected dose (ID) per gram; results are expressed as %ID/gram (±SEM) for N=3 animals. Two-way paired Student-*t* tests were performed comparing values of 60/120 min to values of 30 min: (*) $P \leq 0.05$ and (**) $P \leq 0.01$.

SUPPLEMENT TABLE 4.

Organ Residence Times for ^{68}Ga-NOTA-UBI Estimated from Biodistribution Data in NHP

Organ/ Tissue*	Residence Time (h)	
	Mean	SD
Heart wall	3.55×10^{-3}	3.12×10^{-4}
Brain	1.22×10^{-3}	3.57×10^{-4}
Upper left intestine	9.50×10^{-4}	5.03×10^{-4}
Lower left intestine	6.30×10^{-4}	3.32×10^{-4}
Small intestine	1.58×10^{-3}	8.34×10^{-4}
Stomach	1.05×10^{-3}	2.98×10^{-4}
Kidneys	1.36×10^{-2}	2.91×10^{-3}
Liver	5.97×10^{-2}	1.86×10^{-2}
Lung	2.17×10^{-2}	3.58×10^{-3}
Muscle	8.27×10^{-2}	8.94×10^{-3}
Pancreas	5.73×10^{-4}	1.96×10^{-4}
Red marrow	1.18×10^{-2}	1.90×10^{-3}
Cortical bone	1.01×10^{-2}	2.62×10^{-3}
Spleen	2.23×10^{-3}	4.92×10^{-4}
Testes	1.87×10^{-4}	6.66×10^{-5}
Thyroid	8.80×10^{-5}	5.00×10^{-6}
Blood	5.32×10^{-3}	4.73×10^{-4}
Urine	1.57×10^{-1}	9.54×10^{-2}
Remainder	5.35×10^{-1}	4.70×10^{-2}

*) No residence times could be calculated for adrenals, breast, gallbladder, ovaries, thymus, uterus and trabecular bone.

The Journal of NUCLEAR MEDICINE

^{68}Ga-NOTA-functionalized Ubiquicidin: Cytotoxicity, Biodistribution, Radiation Dosimetry and First-in-Human Positron Emission Tomography/Computed Tomography Imaging of Infections

Thomas Ebenhan, Mike Sathekge, Thabo Lenagana, Michel Koole, Olivier Gheysens, Thavendran Govender and Jan R Zeevaart

J Nucl Med.
Published online: October 19, 2017.
Doi: 10.2967/jnumed.117.200048

The Journal of Nuclear Medicine is published monthly.
SNMMI | Society of Nuclear Medicine and Molecular Imaging
1850 Samuel Morse Drive, Reston, VA 20190.
(Print ISSN: 0161-5505, Online ISSN: 2159-662X)

SNMMI SOCIETY OF NUCLEAR MEDICINE AND MOLECULAR IMAGING